

Structure, Characterization, and Metal-Complexation Properties of a New Tetraazamacrocyclic Containing Two Phenolic Pendant Arms

by **Xiuling Cui**^{a)}, **Maria José Calhorda**^{a) b)}, **Paulo J. Costa**^{a) b)}, **Rita Delgado**^{*a) c)}, **Michael G. B. Drew**^{d)}, and **Vitor Félix**^{e)}

^{a)} Instituto de Tecnologia Química e Biológica, UNL, Apartado 127, P-2781-901 Oeiras
(phone: +351-214 469 737; fax: +351-214 411 277; e-mail: delgado@itqb.unl.pt)

^{b)} Departamento de Química e Bioquímica, Faculdade de Ciências, Universidade de Lisboa, P-1649-016 Lisboa

^{c)} Instituto Superior Técnico, Av. Rovisco Pais, P-1049-001 Lisboa

^{d)} Department of Chemistry, University of Reading, Whiteknights, Reading RG6 6AD, UK

^{e)} Departamento Química, CICECO, Universidade de Aveiro, P-3810-193 Aveiro

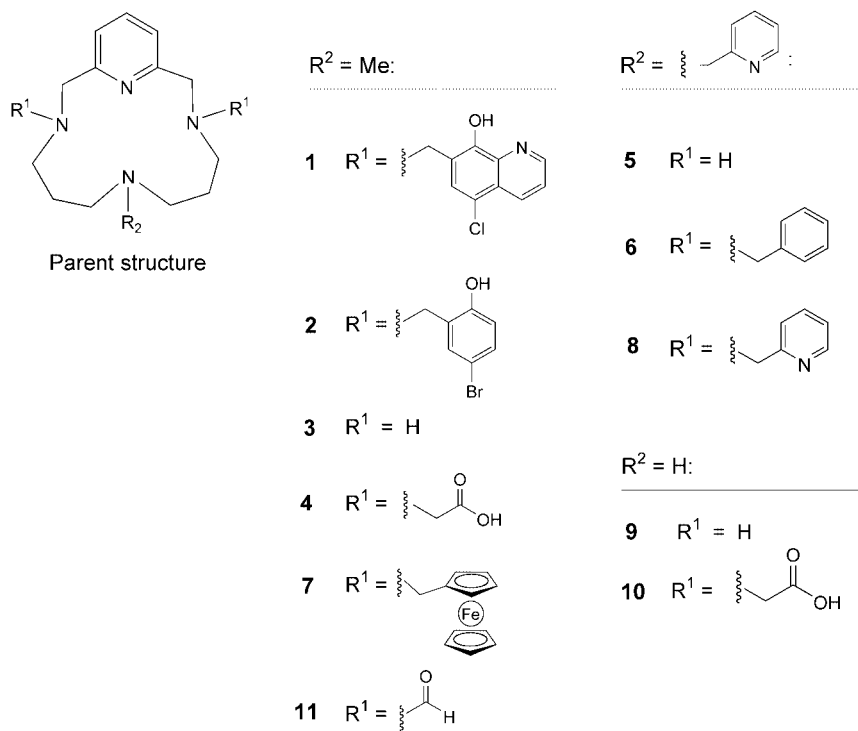
The new tetraazamacrocyclic **2** (=2,2'-[[7-Methyl-3,7,11,17-tetraazabicyclo[11.3.1]heptadeca-1(17),13,15-triene-3,11-diyl]bis(methylene)]bis(4-bromophenol)) was synthesized and used as a ligand for different metal-ion complexes. The X-ray crystal structures of the complexes of the general formula $[M(H-2)]^+NO_3^- \cdot MeOH$ ($M = Ni^{2+}, Zn^{2+}$), in which only one of the two pendant phenolic OH groups of **2** is deprotonated, were determined. In both complexes, the coordination environment is of the [5 + 1] type, the four N-atoms of the macrocyclic framework defining a square-planar arrangement around the metal center, with similar Ni–N and Zn–N distances of 1.961(9) to 2.157(9) Å and 2.021(9) to 2.284(8) Å, respectively. In contrast, the M–O distances are markedly different, 2.060(6) and 2.449(8) Å in the Ni^{II} complex, and 2.027(7) and 2.941(9) Å in the Zn^{II} complex. The UV/VIS spectra of the Ni^{II} and Cu^{II} complexes with ligand **2**, and the EPR spectra of the Cu^{II} system, suggest the same type of structure for the complexes in solution as in the solid state. Theoretical studies by means of density functional theory (DFT) confirmed the experimental structures of the Ni^{II} and Zn^{II} complexes, and led to a proposal of a similar structure for the corresponding Cu^{II} complex. The calculated EPR parameters for the latter and comparison with related data support this interpretation. The singly occupied molecular orbital (SOMO) in these systems is mainly made of a d orbital of Cu, with a strong antibonding (σ^*) contribution of the axially bound phenolate residue.

1. Introduction. – Tetraazamacrocyclics with two or more ionizable pendant arms are able to encapsulate a wide range of divalent and trivalent metal ions of various sizes [1]. The corresponding complexes usually give rise to high stability constants (K_s), and these ligands have become useful in medicinal chemistry, *e.g.*, in the formulation of diagnostic agents or in the design of drugs with antitumor properties [2], as well as in analytical applications [3].

We have recently studied the [14]pyN₃ derivative **1** containing two 5-chloro-8-hydroxyquinoline (CHQ) ligands as pendant arms [4]. The completely deprotonated mononuclear complexes of **1** with several metal ions are formed only at pH > 8, indicating the presence of one basic center on the metal complex. The acidity (in terms of $\log K_a$) was found to be 8.56, 8.58, 9.17, and 9.52 for the corresponding Cu^{II}, Zn^{II}, Cd^{II}, and Pb^{II} complexes, which suggests that protonation is affected by both the size of the metal ions and the stability ($\log K_s$) of the mononuclear complexes [4]. Interestingly, an excess of metal (M) ion relative to the ligand (L) (M/L 2:1) led to complete deprotonation of the complex at much lower pH due to the formation of *dinuclear* complexes. This suggests that, in this case, H⁺ gets trapped by the phenolate O-atom of

CHQ, the most-basic center of the ligand. However, it is puzzling to think that only one of the two phenolates is protonated at high pH.

The aim of the present work was to address the above structural problem by slightly modifying the macrocyclic ligand and to analyze the behavior of the resulting complexes. To achieve this, the two CHQ ligands in **1** were replaced by shorter (4-bromo-2-hydroxyphenyl)methyl moieties, which resulted in formation of macrocycle **2**. Various complexes of **2** were then investigated by UV/VIS, EPR, and X-ray analysis, as well as by DFT calculations to rationalize the structural aspects and spectroscopic data.



2. Results and Discussion. – 2.1. *Synthesis.* Hydroxylated benzyl substituents are usually reacted with azacompounds in the form of halomethyl-substituted phenols [5]. However, a modified *Mannich* reaction, introduced by *Lukyanenko et al.* [6], was used to synthesize **2**. The parent macrocycle **3** (= 7-methyl-3,7,11,17-tetraazabicyclo[11.3.1]-heptadeca-1(17),13,15-triene; Me[14]pyN₃) was reacted in the presence of both paraformaldehyde and the corresponding substituted phenol in benzene, in analogy to [7 – 9]. Although *ortho*-substitution in phenols is preferred over *para*-substitution, the latter position was blocked with a Br-atom to avoid side reactions. The selection of the solvent is crucial for the success of the reaction [8]. The previous preparation of the 3,11-bis(methoxymethyl) derivative of **3** and a one-pot reaction were tried, the former leading to better yield [7]. The resulting compound **2** was subsequently used in the preparation of the corresponding Ni^{II}, Zn^{II}, and Cu^{II} complexes.

2.2. *UV/VIS Spectroscopic Studies.* The UV/VIS/near-IR spectral data of $[\text{Ni}^{\text{II}}\text{-}\mathbf{2}]^0$ and $[\text{Cu}^{\text{II}}\text{-}\mathbf{2}]^0$ are collected in *Table 1*. The electronic spectrum observed for the pale yellow solution of $[\text{Ni}^{\text{II}}\text{-}\mathbf{2}]^0$ shows six well-defined bands of low intensity, characteristic of a tetragonal (D_{4h}) symmetry [10][11]. Following the considerations of *Busch* and co-workers [11] for a large series of tetraazamacrocycles, we tentatively assigned these bands to the two transitions ${}^3\text{B}_{1g} \rightarrow {}^3\text{B}_{2g}$, which is directly related to $10Dq^{xy}$, and ${}^3\text{B}_{1g} \rightarrow {}^3\text{E}_g^a$, which is equal to the difference between $10Dq^{xy}$ and $35/(4D_i)$. Thereby, Dq^z is strongly influenced by the in-plane ligand field, and decreases as Dq^{xy} increases. Values of the equatorial and axial ligand field were calculated for Dq^{xy} and Dq^z as = 1277 and 418 cm^{-1} , respectively. The $[\text{Cu}^{\text{II}}\text{-}\mathbf{2}]^0$ complex exhibited UV/VIS bands at 614 and 430 nm. Upon doubling the amount Cu^{2+} , the longer-wavelength band was shifted to 644 nm, and the molar absorptivity of both bands increased (*Table 1*).

Table 1. *UV/VIS/Near-IR Spectral Data of Selected Ni^{II} and Cu^{II} Complexes of the Ligand 2.* Recorded at 20° in MeOH; λ_{max} in nm, ϵ in $\text{M}^{-1} \text{cm}^{-1}$.

Complex	Stoichiometry	Color	λ_{max} (ϵ)
$[\text{Ni}^{\text{II}}\text{-}\mathbf{2}]^0$	Ni/ 2 1 : 1	Pale yellow	265 (391.6), 324 (263), 380 (sh, 95.2), 561 (10.3),
	Ni/ 2 2 : 1	Pale yellow	783 (11.6), 851 (sh, 7.1), 966 (7.1), 1180 (10)
$[\text{Cu}^{\text{II}}\text{-}\mathbf{2}]^0$	Cu/ 2 1 : 1	Turquoise	430 (146), 614 (203)
	Cu/ 2 2 : 1	Green	422 (242), 644 (269)

2.3. *X-Ray Single-Crystal Structure Analyses.* The X-ray crystal structures of the two complexes $[\text{Ni}^{\text{II}}(\text{H-}\mathbf{2})]\text{NO}_3 \cdot \text{MeOH}$ ¹⁾ and $[\text{Zn}^{\text{II}}(\text{H-}\mathbf{2})]\text{NO}_3 \cdot \text{MeOH}$ are shown in *Fig. 1*. Both compounds were found to be isomorphous. In both cases, the asymmetric unit comprises one $[\text{M}(\text{H-}\mathbf{2})]^+$ cation, one NO_3^- counter ion, and one MeOH solvent molecule (crystallization solvent). The charge balances of the molecular formulae for these two complexes require the protonation of only one donor atom of **2**. Indeed, the X-ray structures unequivocally showed that the pertinent H-atom is bound to the O-atom of only *one* of the two pendant arms (see *Exper. Part*). A H-bond between this phenolic OH group and the NO_3^- anion was observed, with an intermolecular O–H \cdots N distance (angle) of 1.91 Å (140°), respectively, for $[\text{Ni}^{\text{II}}(\text{H-}\mathbf{2})]^+$, and 1.81 Å (175°) for the corresponding Zn^{II} complex. No other significant intermolecular interactions were found, suggesting that, except for the H-bonds mentioned, the crystal lattices are assembled by weak packing interactions.

In both X-ray crystal structures, large anisotropic thermal displacements were found for the three C-atoms bonded to N(7), suggesting that the macrocycle is disordered. However, from the *Fourier* difference maps successively calculated for $[\text{Ni}^{\text{II}}(\text{H-}\mathbf{2})]^+$ and $[\text{Zn}^{\text{II}}(\text{H-}\mathbf{2})]^+$, alternative positions for these atoms were not evident and, consequently, all attempts to find a disorder model were unsuccessful. Therefore, the refinement model used reveals only *thermal* disorder.

¹⁾ The abbreviation 'H-2' means that only one of the two phenolic O-atoms of the pendant arms of the ligand is deprotonated.

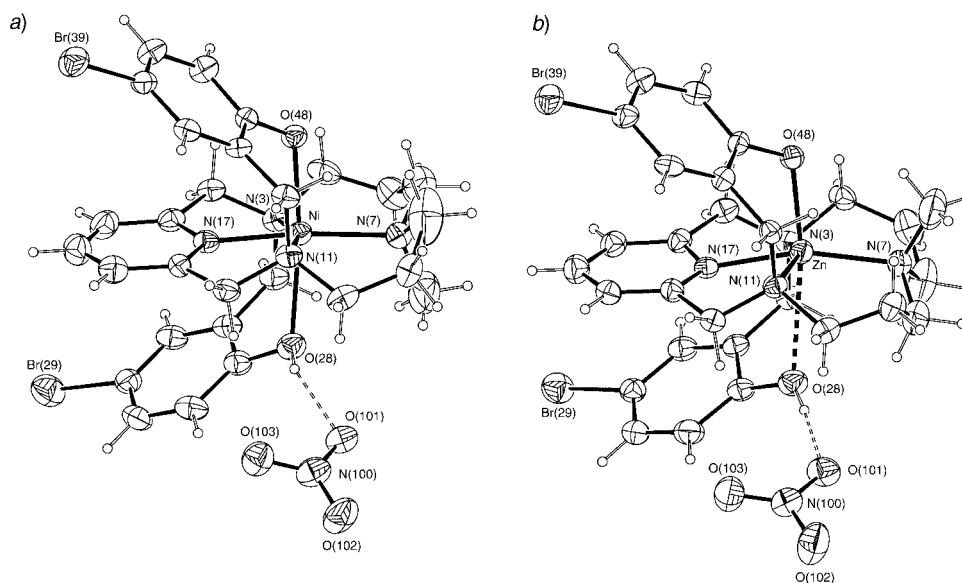


Fig. 1. X-Ray crystal structures of a) $[\text{Ni}^{\text{II}}(\text{H-2})]^+\text{NO}_3^-$ and b) $[\text{Zn}^{\text{II}}(\text{H-2})]^+\text{NO}_3^-$. The ORTEP thermal ellipsoids are drawn at the 20%-probability level. The O–H \cdots N H-bonding interactions between phenolic OH groups and nitrate anions are marked with dashed lines.

The bond distances and angles of $[\text{M}^{\text{II}}(\text{H-2})]^+\text{NO}_3^-$ are listed in Table 2. The data indicate that the coordination environment is of the $[5 + 1]$ type in both complexes ($\text{M} = \text{Ni}^{2+}$, Zn^{2+}). Furthermore, in both cases, the N-atoms of the macrocycle are arranged in a square-planar geometry around the metal center, with the Ni–N and Zn–N distances ranging from 1.961(9) to 2.157(9), and from 2.021(9) to 2.284(8) Å, respectively. In spite of the identical dispositions of the electron-donating N-atoms in these two complexes, the distances between the axial O-atoms of the two phenolic functions and the metal centers are substantially different (2.060(6) and 2.449(8) Å for $\text{M} = \text{Ni}^{2+}$ vs. 2.027(7) and 2.941(9) Å for $\text{M} = \text{Zn}^{2+}$), which reflects the difference between the OH (protonated) and O^- (deprotonated) functions.

The coordination polyhedron of both complexes can be described as an octahedron strongly distorted along the axial coordination axis. The axial angle O–Ni–O of $171.5(3)^\circ$ deviates by only *ca.* 8° from the ideal value (180°). In $[\text{Zn}^{\text{II}}(\text{H-2})]^+\text{NO}_3^-$, the O(28)-atom is also directed towards Zn^{2+} , but at a much longer distance, suggesting square pyramidal rather than octahedral geometry, with the O-atom of the second arm occupying the apex. Furthermore, as would be expected for this type of coordination polyhedron, Zn^{2+} lies above the tetraaza basal plane (0.228(4) Å towards O(48)), leading to an apical Zn–O short distance of $2.027(7)^\circ$. The distance of this O-atom from the mean least-squares plane defined by the four basal N-atoms is only 2.308(9) Å. In contrast, in the corresponding Ni^{II} complex, the metal protrudes by only 0.089(4) Å from this plane. In the Zn^{II} complex, the metal forms an angle of $168.1(3)^\circ$ with the two phenolic O-atoms, which is similar to that found for the Ni^{II} complex. In addition, the $\text{C}(\text{sp}^2)\text{–O–M}$ angle is $115.6(6)^\circ$ for $\text{M} = \text{Ni}^{2+}$, and $111.4(6)^\circ$ for $\text{M} =$

Table 2. Selected Bond Lengths and Angles for the Crystallographically Derived Structures of Two Metal Complexes of the Type $[M^{\text{II}}(\text{H-2})]\text{NO}_3 \cdot \text{MeOH}^{\text{I}}$. See also Fig. 1.

	Bond length [Å]			Bond angle [°]	
	M = Ni ²⁺	M = Zn ²⁺		M = Ni ²⁺	M = Zn ²⁺
M–N(3)	2.157(9)	2.284(8)	O(28)–M–O(48)	171.5(3)	168.1(3)
M–N(7)	2.091(9)	2.061(10)	N(7)–M–N(3)	99.9(4)	98.5(4)
M–N(11)	2.144(9)	2.199(9)	N(11)–M–N(3)	160.9(3)	154.3(3)
M–N(17)	1.961(9)	2.021(9)	N(17)–M–N(3)	80.1(3)	77.6(3)
M–O(48)	2.060(6)	2.027(7)	O(48)–M–N(3)	91.3(3)	98.4(3)
M–O(28)	2.449(8)	2.941(9)	O(48)–M–N(11)	92.0(3)	94.3(3)
			O(48)–M–N(7)	94.6(3)	95.3(3)
			N(7)–M–N(11)	98.6(4)	100.7(4)
			N(17)–M–N(7)	174.0(3)	163.0(4)
			N(17)–M–N(11)	81.0(4)	79.1(3)
			N(17)–M–O(48)	91.4(3)	101.7(3)
			C(27)–O(28)–M	115.6(6)	111.4(6)

Zn²⁺, indicating that, in both cases, one lone-pair electron has a suitable orientation to interact with the metal center.

It is interesting to compare the structure of $[\text{Ni}^{\text{II}}(\text{H-2})]^+\text{NO}_3^-$ with that found for the structurally related Ni^{II} complex of **4**, which contains carboxymethyl substituents in the 3- and 11-positions [13]. The latter displays a distorted octahedral geometry, with four N-atoms determining a square-planar arrangement around the metal center. The O-atoms occupy the axial positions, with Ni–O distances of 2.095(5) and 2.090(5) Å, which is slightly longer than the shortest axial distance reported for $[\text{Ni}^{\text{II}}(\text{H-2})]^+\text{NO}_3^-$; the O–Ni–O axial angles, however, are similar in both complexes (171.5 vs. 175.2° (**4**)). In **4**, the macrocycle is also monoprotonated. Unfortunately, the corresponding *Fourier* difference map did not reveal the position of this H-atom; however, it is probably located on one of the free O-atoms of the carboxylate groups.

Three more X-ray single-crystal structures of Zn^{II} complexes of azamacrocycles of the [14]pyN₃ type with pendant arms were found in the *Cambridge Structural Data Base* [14]. The first two are the mononuclear Zn^{II} complexes of **5** [15] and **6** [16], which display distorted square-pyramidal coordination environments, with the four basal N-atoms defining the equatorial coordination plane. As reported for $[\text{Zn}^{\text{II}}(\text{H-2})]^+\text{NO}_3^-$, the Zn²⁺ ion lies above the equatorial plane, pointing towards the N-atom of the apical pyridylmethyl arm. The third compound, the mononuclear Zn^{II} complex of **7** [17], also exhibits a distorted square-pyramidal geometry, but the macrocycle adopts a folded conformation. Here, atoms N(3), N(7), and N(11) of the macrocycle, together with one I-atom, define the basal plane of the complex, while the N(7)-atom opposite to the pyridine ring occupies the apical position.

In complexes $[\text{M}^{\text{II}}(\text{H-2})]^+\text{NO}_3^-$, the Ni–N and Zn–N distances follow the usual pattern found for tetraazamacrocycles containing a pyridine moiety, *i.e.*, the M–N(sp²) distance is shorter than in M–N(sp³)-type complexes. In addition, the Zn–N(sp²) and Zn–N(sp³) distances (2.021(9) Å and 2.181 Å) compare well with those found for the related complexes of **5–7** [15–17]. The same is true when the Ni–N distances of the corresponding Ni complexes are compared, the Ni–N(sp²) and Ni–N(sp³) average

distances being 1.961(9) and 2.131 Å, respectively, relative to 1.972 Å and 2.102 Å, for the Ni^{II} complex of **4** [13].

In complexes [Ni^{II}(H-2)]⁺NO₃⁻ and [Zn^{II}(H-2)]⁺NO₃⁻, the metal is encapsulated by the macrocycle in a planar conformation, with two pendant arms oriented *trans* to each other, but in a different overall geometry, as can be seen from *Fig. 1*. In the Ni^{II} complex (*Fig. 1, a*), the *N*-Me group lies below the basal coordination plane, and on the same side of the pendant arm positioned at the longest distance from the metal, which gives rise to a (-, -, +) macrocycle conformation²⁾. In the corresponding Zn^{II} complex, the *N*-Me group lies above that plane, leading to a geometric isomer of (-, +, +) configuration [18]. The fitting of atomic coordinates of the macrocycle (excluding the H-atoms) retrieved from the two complexes gave an rms (root mean-square) value of 0.30 Å, which could be reduced to 0.10 Å when only the non-H-atoms of the macrocyclic framework were taken into account. Therefore, in these two complexes, the macrocycles adopt the same conformation.

Another structural feature of [Ni^{II}(H-2)]⁺NO₃⁻ and [Zn^{II}(H-2)]⁺NO₃⁻ is that, in both complexes, the pyridine ring is basically 'sandwiched' between the two aromatic rings of the pendant arms. The pyridine ring forms with the *phenol* ring a dihedral angle of 37.6(4)° (M = Ni²⁺) and 35.6(4)° (M = Zn²⁺), and the corresponding dihedral angle between the pyridine and the *phenolate* ring is reduced to 29.8(4)° and 27.4(5)°, respectively. In spite of the different distances between the O-atom donors of the side arms and the metal center in each complex, they strictly determine the orientation of the pendant arms.

A comparable situation was found in the related (pyridin-2-yl)methyl-appended mononuclear Cu^{II} complex of **8** [19], which also has a [5 + 1] coordination environment. Here, the macrocycle adopts a folded conformation, with the N-atom of the macrocyclic framework *trans* to its pyridine ring occupying the apical position of a distorted square pyramid. One of the pendant arms next to the pyridine ring of the macrocyclic framework is in an equatorial coordination plane, giving rise to a Cu–N distance of 2.043(7) Å, while the second is roughly parallel to the pyridine ring (dihedral angle of 18.3°). Moreover, the N-atom of the second pendant arm is directed towards the Cu²⁺ center, with a Cu⋯N distance of 3.304 Å, which also suggests a weak bonding interaction consistent with a [5 + 1] coordination. The remaining third (pyridin-2-yl)methyl pendant arm is not parallel to the macrocyclic pyridine ring and is further away from the metal center.

2.4. DFT Structural Studies. Several features of the Ni^{II} and Zn^{II} complexes are intriguing, especially their distorted octahedral geometry and the presence of just *one* deprotonated phenol moiety in the pendant arms. It is also interesting that the macrocyclic framework displays different arrangements (configurations) in the Zn^{II} and Ni^{II} complexes, termed *A* and *B*, respectively (see *Fig. 2*, below). To shed light on these phenomena, density-functional-theory (DFT) calculations [20] were carried out with the ADF program [21] (see *Exper. Part*). Full-geometry optimizations were performed for both Zn and Ni, in both the *A* and *B* arrangements (*Fig. 2*).

²⁾ Plus (+) and minus (-) mean that the N-substituent lies above (+) and below (-) the N₄ plane, respectively.



Fig. 2. DFT-Optimized Structures of the $[\text{Ni}^{\text{II}}(\text{H-2})]^+$ complex. The complex is drawn for two different ligand configurations A (left) and B (right). The doubly instead of singly deprotonated system $[\text{Ni}^{\text{II}}\text{-2}]^0$ is also shown (middle¹⁾).

The experimentally observed geometry (X-ray structure) was calculated to be the most stable in each case, although the differences were very small. Configuration B of the Ni^{II} complex was more stable by $0.2 \text{ kcal mol}^{-1}$ than configuration A, and configuration A of the Zn^{II} complex was more stable by $0.6 \text{ kcal mol}^{-1}$ than B. These differences are too small to be traced to a specific feature. However, the agreement between calculated and observed structures is extremely good. Indeed, calculated rms values (for all non-H-atoms) between X-ray and calculated structures were 0.23 \AA for the Zn^{II} and 0.20 \AA for the Ni^{II} complexes, respectively. When the same rms calculation was repeated, taking into account only the metal and its co-ordination sphere (seven instead of 37 atoms), the rms values drop even further to 0.21 \AA (Zn) and 0.17 \AA (Ni), indicating that the structures diverge more in the periphery of the molecules than in the central parts. Such an agreement is not too surprising, given the known accuracy of DFT calculations for these types of fairly rigid complexes, although the size of these systems is relatively large and the Ni species offers the extra challenge of being paramagnetic (two unpaired electrons). On the other hand, if we take these same seven atoms (the metal and six donor atoms), the rms value between the experimental Ni structure and the one calculated for the Zn arrangement is 0.24 \AA , while the opposite (experimental Zn structure vs. Zn in a DFT-optimized Ni environment) is 0.16 \AA . This means that, although the two arrangements differ, the coordination sphere is barely affected, as further reflected by very similar calculated relative energies (ΔE) for both forms (Table 3).

The M–N and M–O distances do not change significantly as one moves from Ni to Zn (despite the two extra electrons in antibonding orbitals), except for one of the M–N_{cis}) and the M–O(H) bonds³⁾, which are significantly longer in the Zn^{II} complex. However, these distances remain long when Ni is introduced into the Zn structure (Table 3, column $[\text{Ni}^{\text{II}}(\text{H-2})]^+$, A), probably due to the influence of the Me substituent.

The most-interesting parameters in these complexes are certainly the axial M–O bonds. The M–O(–) bond for the phenolate residue is significantly shorter than the

³⁾ N_{cis} and N_{trans} refer to N-atoms *cis* and *trans* to the pyridine N-atom, resp.

Table 3. Relative Energies (ΔE , in kcal mol⁻¹) and Selected Distances [\AA] and Angles [$^\circ$] of the DFT-Optimized Structures of Different Ni^{II} and Zn^{II} Complexes. For configurations A vs. B, see Fig. 2.

Complex Configuration	[Ni(H-2)] ⁺		[Ni ^{II} -2] ⁰	[Zn(H-2)] ⁺		[Zn ^{II} -2] ⁰	[Zn ^{II} (H-2)] ⁺ NO ₃ ⁻
	B	A	B	A	B	A	
ΔE	0.0	0.16	–	0.0	0.63	–	–
M–N(py)	1.96	1.95	1.96	2.04	2.03	2.05	2.02
M–N _{trans} ³)	2.11	2.10	2.14	2.11	2.11	2.14	2.40
M–N _{cis}	2.19	2.24	2.15	2.44	2.30	2.25	2.10
M–N _{cis}	2.17	2.15	2.19	2.21	2.22	2.23	2.18
M–O	2.01	2.01	2.16	1.95	1.97	2.13	2.00
M–O(H)	2.93	3.15	2.13	3.59	3.42	2.17	3.05
C–O–M	115.9	116.6	117.7	113.7	114.1	116.7	113.2
C–O(H)–M	107.2	105.0	115.8	103.1	104.1	118.2	111.8

M–O(H) bond, as might be expected, and is shorter in the X-ray structure than in the DFT-calculated one, which probably reflects the role of packing forces and H-bonds in the crystal. The phenolic OH group is involved in one H-bond with the neighboring counter ion (Fig. 1, a). When the geometry was optimized in the presence of the NO₃⁻ ion, the distances did not change much (Table 3), but the Ni–O(H) bond was shortened by 0.5 \AA . The most-significant difference arises from the orientation of the phenyl group involved in the interaction. The new position implies some rearrangements in the peripheral atoms, although the coordination sphere of the metal is barely changed. The calculated O–H distance increases from 0.95 \AA in the isolated ion to 1.05 \AA in the presence of the counter ion. The O–H \cdots O contact is 1.489 \AA long, with an O \cdots O distance of 2.514 \AA and an O–H \cdots O angle of 163 $^\circ$.

To find an answer to this point, the geometry of the doubly deprotonated species [M^{II}-2]⁰ was fully optimized, using the preferred arrangement in each case, for the Ni (B) and Zn (A) derivatives. The optimized geometry of the [Ni^{II}-2]⁰ complex is also shown in Fig. 2. It can be seen that the original M–O(H) bond is shortened considerably, the two new M–O(–) bonds now adopting values between 2.10 and 2.15 \AA , which is perfectly consistent with a ‘normal’ Ni–O or Zn–O bond. The rms values for the DFT-optimized [M^{II}-2]⁰ structures and the X-ray is 0.23 \AA for M = Ni, and 0.40 \AA for M = Zn, when considering all 37 non-H-atoms. These values essentially reflect the approach of the additional phenolate O-atom to the metal, the rest of the molecule being unperturbed.

2.5. Experimental and Theoretical EPR Studies. The electron-paramagnetic-resonance (EPR) spectrum of the Cu^{II} complex of **2** was recorded in a H₂O/DMSO 1:1 mixture. In the case of a 1:1 metal-to-ligand ratio, the spectrum indicated the presence of two species (A and B), as easily observed by the splitting of the bands at low field. Taking into account the similarity of this spectrum with that of the Cu^{II} complex of **1** carried out under the same experimental conditions [4], the species A and B can be attributed to [M^{II}(H-2)]⁺ and [M^{II}-2]⁰ complexes. Each species exhibited three well-resolved lines at low field, and no superhyperfine splitting. The strong, unresolved band in the high-field region of the EPR spectrum overlaps the fourth line. The hyperfine coupling constants and *g* values of glassy solutions of these complexes, obtained by simulation of the spectrum [22], are compiled in Table 4, together with

Table 4. EPR Data of Different Cu^{II} Complexes. The tensors g and A are expressed in terms of 10^4 cm^{-1} . Recorded at 102–130 K in DMSO/H₂O. For ligands, see chemical formulae.

Complex	λ_{max} [nm]	Species	g_x	g_y	g_z	A_x	A_y	A_z	Source
[Cu-2] ⁰	614	<i>A</i>	2.049	2.068	2.229	13.6	13.5	178.1	a)
		<i>B</i>	2.050	2.060	2.194	3.0	11.3	163.8	a)
[Cu-3] ²⁺	560 ^{b)}		2.039	2.080	2.201	4.9	14.7	195.9	[17]
[Cu-9] ²⁺	560		2.034	2.060	2.188	0.5	3.4	192.9	[23]
[Cu-7] ²⁺	600 ^{b)}		2.032	2.074	2.199	0.8	17.2	170.3	[17]
[Cu-10] ⁰	614		2.034	2.080	2.209	14.3	8.5	167.1	[24]
[Cu-4] ⁰	630		2.027	2.084	2.221	14.9	21.3	165.4	[23]

a) This work. b) In DMF.

those of other Cu^{II} complexes based on the same macrocyclic framework, but with different pendant arms [13][17][23][24]. The parameters of these species are typical of Cu^{II} complexes of an axially elongated rhombic symmetry, and with a $d_{x^2-y^2}$ ground state, consistent with elongated rhombic-octahedral or distorted square-based pyramidal configurations [25].

From EPR spectroscopy and the ligand-field theory, it is known that the addition of axial ligands to a square-planar complex decreases A_z , but increases g_z , with a simultaneous red-shift in the electronic spectra [26]. In agreement with this, the EPR spectrum of the square-planar Cu^{II} complex of the unsubstituted macrocycle **9**, *i.e.*, [Cu^{II}-**9**]²⁺, for which an X-ray crystal structure is available [18], shows lower g_z and higher A_z values, in combination with a blue-shifted band of the maximum VIS absorption [23]. This is in contrast to the corresponding values for [Cu^{II}-**7**]²⁺ and [Cu^{II}-**10**]⁰, which exhibit distorted square-pyramidal and octahedral geometries, respectively [17][24]. The basal planes of the last two complexes are formed by the four N-atoms of the macrocycle, and the fifth position of [Cu^{II}-**7**]²⁺ is occupied by a Cl-atom, while the six-coordination of [Cu^{II}-**10**]⁰ is completed *via* the two O-atoms of the appended carboxylate groups, as shown by the X-ray structures.

The EPR parameters of both species *A* and *B* of the Cu^{II} complex of **2** are similar to those of [Cu-**7**]²⁺ and [Cu-**10**]⁰, indicating that both complexes are penta- or hexacoordinated. However, the g_z values for species *A* is higher than expected for a square-pyramidal geometry, and that of species *B* is lower than expected for an octahedral environment.

DFT Calculations have been used in recent years to compute EPR parameters, which can be compared to the experimental data. This is a complementary approach to the classic ligand-field theory, which does neither directly include covalent bonds nor allow for mixing of d orbitals, when the symmetry is lowered from the octahedral group (O_h) [27]. Therefore, an attempt was made to predict the structure of [Cu^{II}-**2**]⁰, as no crystal structure was available. Experimental evidence suggested a structure similar to those of the corresponding Ni^{II} and Zn^{II} complexes. Since this type of complex is paramagnetic, and, because the difference between the Ni and Zn forms is very small, the geometry was optimized starting from the Ni structure (configuration *B*). The optimized geometry of [Cu^{II}(H-**2**)]⁺ is shown in *Fig. 3, a*. Once again, the M–O(–) bond is much shorter than the M–O(H) bond (2.14 vs. 3.20 Å, resp.), while the Cu–N

bonds are comparable in size to those in the previous species. This complex, therefore, adopts a geometry that can be considered a mixture between distorted octahedral and square pyramidal. The metal does not lie in the plane of the N-atoms, protruding toward the phenolate side. The unpaired electron in this d^9 complex occupies an orbital of mainly d_z^2 type (SOMO), with a strong contribution from the phenolate arm, as can be seen in *Fig. 3, b*.

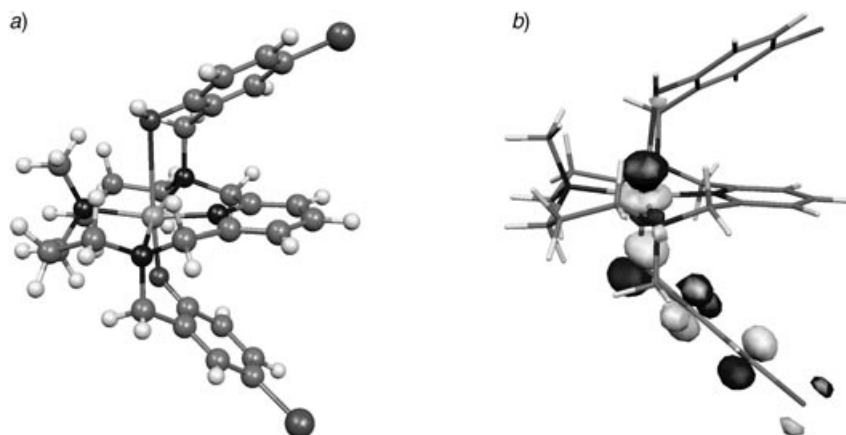


Fig. 3. a) DFT-Calculated structure of the $[\text{Cu}^{\text{II}}(\text{H-2})]^+$ complex and b) the corresponding singly occupied molecular orbital (SOMO)

The calculated spin density of $[\text{Cu}^{\text{II}}(\text{H-2})]^+$ is concentrated on Cu^{2+} (42.1%), with contributions from the N-atoms (*ca.* 6% each), the phenolate O-atom (9.2%), and C-atoms from the adjacent phenyl ring (4.8, 7.2, and 5.6%).

To calibrate our DFT-calculated EPR data, the more-octahedral $[\text{Cu}^{\text{II}}\text{-10}]^0$ complex (see *Table 4*) was also analyzed based on the crystal-structure coordinates (for details, see the *Exper. Part*). Here, the metal is bound to four N-atoms in the equatorial plane, and to two axial O-atoms from the carboxylate groups (*Fig. 4, a*), and the experimental geometry could be nicely reproduced.

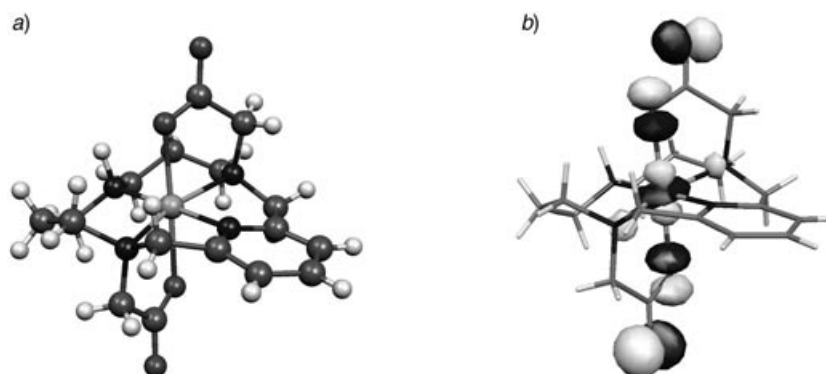


Fig. 4. DFT-Calculated structure of a) the $[\text{Cu}^{\text{II}}\text{-10}]^0$ complex and b) the corresponding singly occupied molecular orbital (SOMO)

In $[\text{Cu}^{\text{II}}\text{-10}]^0$, the spin density is also mainly concentrated on Cu (52.4%), with contributions from the N-atoms (7.0% for the pyridine N-atom, and 7.4, 9.2, and 10.0% for the others, resp.), and the carboxylate O-atoms (4.5 and 3.6%). The calculated singly occupied molecular orbital (SOMO; Fig. 4, b) shows a strong contribution of $\text{Cu}(x^2 - y^2)$, with some mixing of the z^2 orbital, and is σ^* antibonding toward the axial O-atoms. The apparent discrepancy between the large contribution of N-atoms to the spin density and their absence from the SOMO reflects the importance of internal levels and spin-polarization effects. The latter are also responsible for the splitting of the levels in a spin-unrestricted calculation when compared to the results of a spin-restricted one, as shown in Fig. 5 for the above two Cu^{II} complexes, i.e., $[\text{Cu}^{\text{II}}(\text{H-2})]^+$ and $[\text{Cu}^{\text{II}}\text{-10}]^0$.

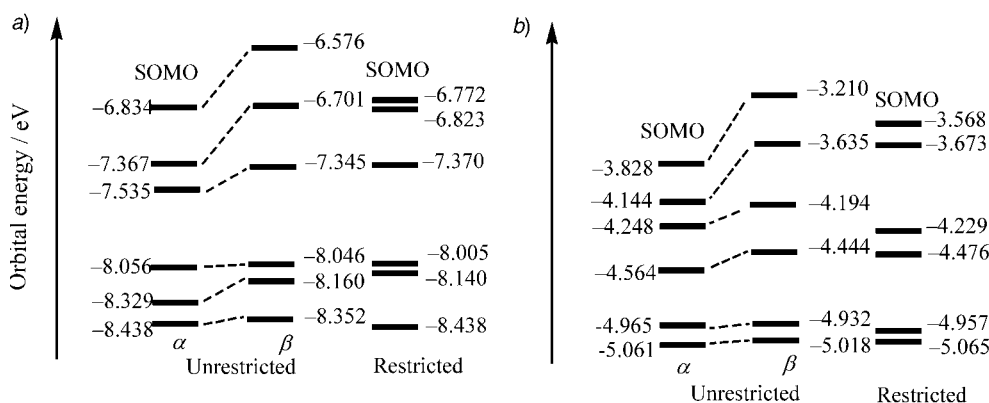


Fig. 5. Calculated energy diagram of the frontier orbitals of the complexes a) $[\text{Cu}^{\text{II}}(\text{H-2})]^+$ and b) $[\text{Cu}^{\text{II}}\text{-10}]^0$

The electronic-transition energy estimated from the calculated molecular-orbital (MO) levels, based on one-electron excitations ending at the SOMO, differs strongly from the experimental results, as has been observed before for other Cu^{II} complexes [27]. However, upon performing TD-DFT calculations with Gaussian98 [28], the most-intense UV/VIS bands were found to be at 684 and 512 nm, as compared to experimental values of 614 and 430 nm, respectively (see Table 1). The agreement is even better when we consider that both bands are equally shifted to higher wave numbers, which confirms the structural assignment (Fig. 3). The band at 512 nm corresponds to a pure $d \rightarrow d$ transition, while the one at 684 nm arises from a mixture of $d \rightarrow d$ contribution and interligand charge transfers.

The calculated EPR parameters for $[\text{Cu}^{\text{II}}(\text{H-2})]^+$ and $[\text{Cu}^{\text{II}}\text{-10}]^0$ are presented in Table 5. Some general statements can be drawn: 1) the influence of the basis set on the results is small (the B1 set is of lower quality than the default one, and B2 is better; in all other cases, the standard basis set was used; see *Exper. Part*), and the effect of changing the substituent R^2 at N(7) from Me to H (see chemical formulae) is also negligible. 2) With respect to the g values, there are significant discrepancies between the calculated and experimental data, as has been described in other calculations [29]. 3) The patterns of the EPR A values also exhibit a large deviation, A_z being much larger than all the others for both complexes. The calculated A values usually tend to deviate stronger

Table 5. DFT-Calculated and Experimental EPR Parameters of Two Cu^{II} Complexes. The tensors *g* and *A* are expressed in terms of 10⁴ cm⁻¹.

Complex	<i>g_x</i>	<i>g_y</i>	<i>g_z</i>	<i>A_x</i>	<i>A_y</i>	<i>A_z</i>	Source
[Cu ^{II} (H-2)] ⁺	2.049	2.068	2.229	13.6	13.5	178.1	a)
	2.050	2.060	2.194	3.0	11.3	163.8	b)
	2.013	2.067	2.106	3.8	53.4	95.2	c)
	2.010	2.069	2.103	2.8	54.8	96.6	d)
[Cu ^{II} -10] ⁰	2.034	2.080	2.209	14.3	8.5	167.1	[24]
	1.998	2.063	2.097	29.2	32.0	115.5	c)
	1.998	2.065	2.099	29.3	31.6	115.2	d)

a) This work (A). b) This work (B). c) Basis set B1 (lower quality). d) Basis set B2 (higher quality).

from the experimental values compared to the *g*-tensor components [30]. These deviations result from limitations in the ADF program, and it is, thus, not possible to improve these results.

The solid-state and solution structures of [Cu^{II}-10]⁰ are likely to be very similar. From the DFT results, its structure cannot be distinguished from the Me derivative [Cu^{II}-4]⁰. Therefore, when dealing with the Cu^{II} complex of **2**, the solution species of configuration *B* should have a structure very similar to the one of the corresponding Ni^{II} complex, which was used to model the Cu complex, without applying significant modifications. The coordination geometry is somewhere intermediate between octahedral and distorted square-pyramidal. In both cases, the SOMO consists mainly of a *d* orbital, with a mixed contribution of *x*² – *y*² plus some mixing of *z*² orbitals, but there are also strong contributions of the axial ligands. Another point to be mentioned is the contribution of the equatorial N-atoms to the spin density, although their contribution to the SOMO is negligible. These observations illustrate the limitations of the ligand-field approach in interpreting EPR spectra.

3. Conclusions. – The X-ray crystal structures of the complexes [Ni^{II}(H-2)]⁺NO₃⁻ and [Zn(H-2)]⁺NO₃⁻ show that the macrocycle encapsulates the metal centers in a fashion in which one phenol residue is deprotonated (phenolate), whereas the other is not deprotonated but still points to the Ni²⁺ or Zn²⁺ ions, which is consistent with EPR studies in solution. In the solid state, the ‘free’ phenolic OH group is involved in a H-bond with the NO₃⁻ counter-ion. In aqueous solution, H₂O molecules can easily replace the nitrate anion. DFT Calculations have shown that the calculated and experimentally determined structures generally agree well, the deprotonated complex being also expected to be stable, with two comparable Ni–O bonds. Moreover, since potentiometric studies of various metal complexes of ligand **1** had shown earlier that the residual phenolic OH group is not deprotonated even at high pH, its acidity must be intrinsically tuned by its stereoelectronic disposition in the vicinity of the metal ion. Indeed, the p*K*_a value of [M^{II}(H-1)]⁺ complexes follows the trend Pb > Cd > Zn > Cu, suggesting that the basicity of the coordinated phenolic OH group in complexes with ligands **1** or **2** is the result of a delicate balance between the ligand-field strength, the geometric constraints imposed both by the metal and the ligand, and potential H-bonds

between this OH group and solvent molecules or counter-ions. All together, these effects favor a [5 + 1] coordination geometry over a perfect octahedral arrangement.

An interpretation of the EPR spectrum of $[\text{Cu}^{\text{II}}(\text{H-2})]^+$ was attempted. Full-geometry optimization of a model based on the structure of the corresponding Ni^{II} complex led to a geometry similar to the one described above, with a coordination between square-pyramidal and octahedral. The calculated EPR *g*- and *A*-tensor components showed large deviations from those determined experimentally. The calculation of the related complex $[\text{Cu-10}]^0$, with a more-symmetric, tetragonally distorted octahedral environment (as determined experimentally), allowed the comparison of calculated and experimental results in another system. The differences between the two sets of values are similar, and it is not possible to increase the quality of these calculations. In both cases, the singly occupied molecular orbital (SOMO) is mainly of the d-type, with a mixed contribution of $x^2 - y^2$ and some z^2 orbitals, but with strong antibonding contributions of the axial ligands.

Experimental Part

General. The parent macrocycle **3** (= 7-methyl-3,7,11,17-tetraazabicyclo-[11.3.1]heptadeca-1(17),13,15-triene) was synthesized by previously reported procedures [31]. All chemicals were of reagent grade and used as supplied without further purification.

UV/VIS Spectra were recorded on a *UNICAM UV-4* or (for UV/VIS/near-IR) on a *Shimadzu UV-3100* spectrophotometer in MeOH or DMSO/H₂O 1:1; $\tilde{\nu}$ in cm^{-1} . The samples were prepared by the addition of increasing amounts of metal ion (in the form of nitrate or chloride salts) to the ligands **1–10** at the appropriate pH value. IR Spectra were recorded from KBr pellets on a *UNICAM Mattson-7000* spectrometer. ¹H- and ¹³C-NMR spectra were recorded on a *Bruker AMX-300* spectrometer at 300/75 MHz; chemical shifts δ are given in ppm rel. to Me₄Si by referencing to residual solvent signals. EPR Spectra were recorded on a *Bruker ESP-380* spectrometer equipped with continuous-flow cryostats for liquid N₂, operating at X-band. The EPR spectra of Cu^{II} complexes (1–20 mM) were recorded in the range of 102 to 130 K and 7.5 to 32 K, in DMSO/H₂O mixtures and in 1M tetrabutylammonium nitrate (TBAN) solutions. Computer-simulated EPR spectra were generated with a program for a micro computer [22]. Microanalyses were carried out by the Instituto de Tecnologia Química e Biológica (ITQB) Microanalytical Service.

2,2'-[7-Methyl-3,7,11,17-tetraazabicyclo[11.3.1]heptadeca-1(17),13,15-triene-3,11-diyl]bis(methylene)-bis(4-bromophenol) (**2**). Compound **3** (0.5 g, 2.0 mmol) [31] was treated with formaldehyde (0.165 g, 5.4 mmol) in MeOH (10 ml). After standing overnight at r.t., the solvent was evaporated under reduced pressure, and to the resulting, well-dried intermediate **11** (quant.) was added 4-bromophenol (0.69 g, 4.0 mmol) in benzene (20 ml). The mixture was refluxed for 21 h, cooled down, and evaporated. The resulting residue was purified by column chromatography (CC; SiO₂; CHCl₃/MeOH 20:1) and recrystallization (CH₂Cl₂/hexane 2:1): 0.93 g (74.7%) of **2**. Colorless crystals. M.p. 209–210°. IR (KBr): 3432, 2945, 2850, 2787, 1577, 1479, 1458, 1387, 1269, 1113, 974, 822, 758, 625. ¹H-NMR (CDCl₃): 1.67 (*q*, 4 H, NCH₂CH₂CH₂N); 2.00 (*s*, 3 H, MeN); 2.27 (*br.*, 4 H, NCH₂CH₂); 2.62 (*t*, 4 H, NCH₂CH₂); 3.78 (*s*, 4 H, NCH₂); 3.83 (*s*, 4 H, NCH₂); 6.74 (*d*, *J* = 8.7, 2 pyridyl H); 7.11 (*s*, 2 arom. H); 7.13 (*d*, 2 arom. H); 7.27 (*d*, 2 arom. H); 7.63 (*t*, *J* = 7.6, 1 pyridyl H). ¹³C-NMR (CDCl₃; DEPT): 23.3; 43.3; 50.2; 53.7; 57.9; 58.1; 110.4; 118.0; 122.2; 124.4; 131.2; 131.3; 137.2; 156.5; 156.8. Anal. calc. for C₂₈H₃₄Br₂N₄O₂ · 0.5 H₂O: C 53.59, H 5.62, N 8.93; found: C 53.40, H 5.60, N 8.96.

Preparation of the Complex [Ni^{II}(H-2)]⁺NO₃⁻ · H₂O. An aq. soln. of Ni(NO₃)₂ · 6 H₂O (0.039 g, 0.136 mmol) was added to a stirred soln. of **2** (42 mg, 67.9 μmol) dissolved in a minimum (*ca.* 6 ml) of MeOH/CH₂Cl₂ 1:2. The mixture was stirred for 2 h and then concentrated to dryness. The residue was taken up in MeOH and filtered. From the MeOH filtrate, dark-blue crystals were obtained by slow evaporation (2 d) of the solvent in contact with air. Yield: 90%. Anal. calc. for C₂₈H₃₄Br₂N₅NiO₅ · H₂O: C 44.40, H 4.79, N 9.25; found: C 44.37, H 4.68, N 9.36.

Preparation of the Complex [Zn^{II}(H-2)]⁺NO₃⁻. Prepared as described above for the corresponding Ni^{II} complex, but from Zn(NO₃)₂ (0.016 g, 55.8 μmol) and **2** (34 mg, 55.6 μmol). Yield: 90%. Yellow crystals.

Crystallography. The crystallographic data for $[\text{Ni}^{\text{II}}(\text{H-2})]^+\text{NO}_3^- \cdot \text{MeOH}$ and $[\text{Zn}^{\text{II}}(\text{H-2})]^+\text{NO}_3^- \cdot \text{MeOH}$ are collected in Table 6. The data for these two compounds were collected on an MAR research-image-plate system equipped with graphite-monochromated MoK_α radiation ($\lambda = 0.71073 \text{ \AA}$). A total of 95 frames were measured at 2° intervals using a counting time adequate to the crystal under study. Data analyses were performed with the XDS program [32]. Empirical absorption corrections were applied to the intensities by means of the DIFABS program [33].

Table 6. Room-Temperature Crystallographic Data and Pertinent Refinement Details for the Structures Solved in This Work

$[\text{Ni}^{\text{II}}(\text{H-2})]^+\text{NO}_3^- \cdot \text{CH}_3\text{OH}$	$[\text{Zn}^{\text{II}}(\text{H-2})]^+\text{NO}_3^- \cdot \text{CH}_3\text{OH}$	
Formula	$\text{C}_{29}\text{H}_{37}\text{Br}_2\text{N}_5\text{NiO}_6$	$\text{C}_{29}\text{H}_{37}\text{Br}_2\text{N}_5\text{O}_6\text{Zn}$
M_r	770.17	776.83
Crystal system	Monoclinic	Monoclinic
Space group	$P2_1/c$	$P2_1/c$
Unit cell:		
a [\AA]	10.774(14)	10.870(17)
b [\AA]	22.75(3)	22.83(3)
c [\AA]	13.339(15)	12.983(15)
β [$^\circ$]	100.06(1)	97.99(1)
V [\AA^3]	3219(7)	3191(7)
Z	4	4
D_c [mg m^{-3}]	1.589	1.617
μ [mm^{-1}]	3.134	3.323
Reflections collected	19807	19659
Unique reflections, [R_{int}]	5883, [0.1593]	6176, [0.0628]
R_1, wR_2 ($I > 2\sigma(I)$)	0.0959, 0.2028	0.0924, 0.2780
R_1, wR_2 (all data)	0.2051, 0.2521	0.1314, 0.2951

The merge of the intensity data of the $[\text{Ni}^{\text{II}}(\text{H-2})]^+$ complex in the *Laue* symmetry group $2/m$ led to a higher R_{int} value of 0.1593, suggesting that the crystal used in the data collection had a lower degree of crystallinity. In fact, several crystals of the Ni^{II} complex were investigated, and the image-plate-patterns showed that all of them had fairly poor and weak diffraction patterns. In spite of this experimental drawback, the structure was solved unambiguously, and the quality of the final data was comparable to that for the corresponding Zn^{II} complex.

The structures of $[\text{Ni}^{\text{II}}(\text{H-2})]^+$ and $[\text{Zn}^{\text{II}}(\text{H-2})]^+$ were solved by direct methods and refined by full-matrix least-squares analysis against F^2 , using SHELXS and SHELXL from the SHELX97 package [34]. All non-H-atoms were refined with anisotropic thermal parameters. The H-atoms bonded to C-atoms were inserted in geometric positions, and those attached to O-atoms were localized according to *Fourier* difference maps. The OH H-atoms were introduced in the refinement, assuming O–H distances and H–O \cdots H angles constrained to 0.82 \AA and 104.5° , resp. All atomic H-atom positions were refined, giving rise to an isotropic thermal parameter 1.2 times those of the atoms to which they were bonded. The structures were refined convergence was achieved, leading to R values listed in Table 6. The largest peaks and holes in the final difference *Fourier* maps were 0.684 and -0.355 e\AA^{-3} for the Ni^{II} complex, and 0.960 and -0.521 e\AA^{-3} for the Zn analogue, which is within the values expected.

DFT Calculations. DFT Calculations [20] were performed with the Amsterdam-density-functional program package (ADF) [21]. The local spin density (LSD) exchange correlation potential was used with the local density approximation of the correlation energy [35]. Full-geometry optimizations, without any symmetry constraints, were performed by means of the generalized gradient approximation [36], using *Perdew–Wang* exchange and correlation corrections [37]. Spin-unrestricted calculations were performed for all the Cu^{II} and Ni^{II} paramagnetic complexes studied. The inner shells of Ni^{2+} , Cu^{2+} , and Zn^{2+} ($[1-2]s, 2p$); C, N, and O ($1s$); Br ($[1-3]s, [1-3]p$) were frozen. An uncontracted triple- ζ STO basis set, with one polarization function, was used to describe the valence shells of all elements. For the EPR calculations, all electron basis sets, consisting of uncontracted triple- ζ STO functions, augmented by one polarization function, were used for all elements (unless

otherwise mentioned). The basis set B1 consisted of a double- ζ STO basis with one polarization function; for the B2 basis set, all electron basis sets with uncontracted triple- ζ STO functions, and augmented by two polarization functions, were considered. The ZORA method was used to account for relativistic effects and spin–orbit coupling [38]. The EPR A values were obtained from an unrestricted calculation, and the g values from a spin-restricted calculation with spin–orbit correction.

The starting geometries were taken from the crystal structures of the complexes with the ligand **2** (described in this work) and the published structure of $[\text{Cu}^{\text{II}}\text{-10}]^0$ [24]. Graphical representations of molecular orbitals were drawn with MOLEKEL [39]. TD-DFT [40] Calculations were performed with the Gaussian98 package [28] on the ADF-optimized structure of $[\text{Cu}^{\text{II}}(\text{H-2})]^+$. The unrestricted B3LYP [41] formalism was adopted (10 states were requested). The standard LANL2DZ [42] basis set along with the associated ECP was used for Cu and Br, a standard 6-31G(d) basis set [43] was used for C, O and N, and the 3-21G basis set [44] was taken for H.

R. D. and V. F. acknowledge financial support from *Fundação para a Ciência e Tecnologia (FCT)* and *POCTI*, with co-participation of the EU fund *FEDER* (Project No. POCTI/1999/QUIM/35396). X. C. and P. J. C. acknowledge *FCT* for the grants SFRH/BPD/1502/2000 and SFRH/BD/10535/2002, resp.

REFERENCES

- [1] K. P. Wainwright, *Coord. Chem. Rev.* **1997**, *166*, 35; T. A. Kaden, *Adv. Supramol. Chem.* **1993**, *3*, 65.
- [2] S. Liu, D. S. Edwards, *Bioconjugate Chem.* **2001**, *12*, 7; A. Heppeler, S. Froidevaux, A. N. Eberle, H. R. Maecke, *Curr. Med. Chem.* **2000**, *7*, 971; C. J. Anderson, M. J. Welch, *Chem. Rev.* **1999**, *99*, 2219.
- [3] J. S. Bradshaw, R. M. Izatt, *Acc. Chem. Res.* **1997**, *30*, 338; S. C. Lee, R. M. Izatt, X. X. Zhang, E. G. Nelson, J. D. Lamb, P. B. Savage, J. S. Bradshaw, *Inorg. Chim. Acta* **2001**, *317*, 174.
- [4] X. Cui, M. F. Cabral, J. Costa, R. Delgado, *Inorg. Chim. Acta* **2003**, *356*, 133.
- [5] U. Auerbach, U. Eckert, K. Wieghardt, B. Nuber, J. Weiss, *Inorg. Chem.* **1990**, *29*, 938.
- [6] N. G. Lukyanenko, V. N. Pastushok, A. V. Bordunov, *Synthesis* **1991**, 241; A. V. Bordunov, N. G. Lukyanenko, V. N. Pastushok, K. E. Krakowiak, J. S. Bradshaw, N. K. Dalley, X. Kou, *J. Org. Chem.* **1995**, *60*, 4912.
- [7] X. X. Zhang, A. V. Bordunov, J. S. Bradshaw, N. K. Dalley, X. Kou, R. M. Izatt, *J. Am. Chem. Soc.* **1995**, *117*, 11507.
- [8] K.-W. Chi, H.-C. Wei, T. Kottke, R. J. Lagow, *J. Org. Chem.* **1996**, *61*, 5684.
- [9] A. V. Bordunov, J. S. Bradshaw, X. X. Zhang, N. K. Dalley, X. Kou, R. M. Izatt, *Inorg. Chem.* **1996**, *35*, 7229.
- [10] A. B. P. Lever, 'Inorganic Electronic Spectroscopy', 2nd edn., Elsevier, Amsterdam, 1984; R. W. Renfrew, R. S. Jamison, D. C. Weatherburn, *Inorg. Chem.* **1979**, *18*, 1584; R. Smierciak, J. Passariello, E. L. Blinn, *Inorg. Chem.* **1977**, *16*, 2646.
- [11] L. Y. Martin, C. R. Sperati, D. H. Busch, *J. Am. Chem. Soc.* **1977**, *99*, 2968.
- [12] L. Spek, 'PLATON, a Multipurpose Crystallographic Tool', Utrecht University, Utrecht, The Netherlands, 1999.
- [13] J. Costa, R. Delgado, M. G. B. Drew, V. Félix, R. T. Henriques, J. C. Waerenborgh, *J. Chem. Soc., Dalton Trans.* **1999**, 3253.
- [14] F. H. Allen, *Acta Cryst., Sect. B* **2002**, *58*, 380; I. J. Bruno, J. C. Cole, P. R. Edginton, M. Kessler, C. F. Macrae, P. McCabe, J. Pearson, R. Taylor, *Acta Cryst., Sect. B* **2002**, *58*, 389.
- [15] S. J. Grant, P. Moore, H. A. A. Omar, N. W. Alcock, *J. Chem. Soc., Dalton Trans.* **1994**, 485.
- [16] N. W. Alcock, K. P. Balakrishnan, A. Berry, P. Moore, C. J. Reader, *J. Chem. Soc., Dalton Trans.* **1988**, 1089.
- [17] J. Costa, R. Delgado, M. G. B. Drew, V. Félix, A. Saint-Maurice, *J. Chem. Soc., Dalton Trans.* **2000**, 1907.
- [18] V. Félix, M. J. Calhorda, J. Costa, R. Delgado, C. Brito, M. T. Duarte, T. Arcos, M. G. B. Drew, *J. Chem. Soc., Dalton Trans.* **1996**, 4543.
- [19] J. Costa, R. Delgado, M. G. B. Drew, V. Félix, *J. Chem. Soc., Dalton Trans.* **1999**, 4331.
- [20] R. G. Parr, W. Yang, 'Density Functional Theory of Atoms and Molecules', Oxford University Press, New York, 1989.
- [21] E. J. Baerends, A. Bércecs, C. Bo, P. M. Boerrigter, L. Cavallo, L. Deng, R. M. Dickson, D. E. Ellis, L. Fan, T. H. Fischer, C. Fonseca Guerra, S. J. A. van Gisbergen, J. A. Groeneveld, O. V. Gritsenko, F. E. Harris, P. van den Hoek, H. Jacobsen, G. van Kessel, F. Kootstra, E. van Lenthe, V. P. Osinga, P. H. T. Philipsen, D. Post, C. C. Pye, W. Ravenek, P. Ros, P. R. T. Schipper, G. Schreckenbach, J. G. Snijders, M. Sola, D. Swerhone, G. te Velde, P. Vernooijs, L. Versluis, O. Visser, E. van Wezenbeek, G. Wiesenekker, S. K. Wolff,

- T. K. Woo, T. Ziegler, ADF-2002 program (see www.scf.com); E. J. Baerends, D. Ellis, P. Ros, *Chem. Phys.* **1973**, 2, 41; E. J. Baerends, P. Ros, *Int. J. Quantum Chem.* **1978**, S12, 169; P. M. Boerrigter, G. te Velde, E. J. Baerends, *Int. J. Quantum Chem.* **1988**, 33, 87; G. te Velde, E. J. Baerends, *J. Comput. Phys.* **1992**, 99, 84.
- [22] F. Neese, Diploma Thesis, University of Konstanz, 1993.
- [23] J. Costa, R. Delgado, M. C. Figueira, R. T. Henriques, M. Teixeira, *J. Chem. Soc., Dalton Trans.* **1997**, 65.
- [24] J. Costa, R. Delgado, M. G. B. Drew, V. Félix, *J. Chem. Soc., Dalton Trans.* **1998**, 1063.
- [25] B. J. Hathaway, *Coord. Chem. Rev.* **1983**, 52, 87; H. Yokoi, M. Sai, T. Isobe, S. Ohsawa, *Bull. Chem. Soc. Jpn.* **1972**, 45, 2189.
- [26] P. W. Lau, W. C. Lin, *J. Inorg. Nucl. Chem.* **1975**, 37, 2389; M. J. Maroney, N. J. Rose, *Inorg. Chem.* **1984**, 23, 2252.
- [27] R. Deeth, *J. Chem. Soc., Dalton Trans.* **2001**, 664.
- [28] M. J. Frisch, G. W. Trucks, H. B. Schlegel, G. E. Scuseria, M. A. Robb, J. R. Cheeseman, V. G. Zakrzewski, J. A. Montgomery Jr., R. E. Stratmann, J. C. Burant, S. Dapprich, J. M. Millam, A. D. Daniels, K. N. Kudin, M. C. Strain, O. Farkas, J. Tomasi, V. Barone, M. Cossi, R. Cammi, B. Mennucci, C. Pomelli, C. Adamo, S. Clifford, J. Ochterski, G. A. Petersson, P. Y. Ayala, Q. Cui, K. Morokuma, N. Rega, P. Salvador, J. J. Dannenberg, D. K. Malick, A. D. Rabuck, K. Raghavachari, J. B. Foresman, J. Cioslowski, J. V. Ortiz, A. G. Baboul, B. B. Stefanov, G. Liu, A. Liashenko, P. Piskorz, I. Komaromi, R. Gomperts, R. L. Martin, D. J. Fox, T. Keith, M. A. Al-Laham, C. Y. Peng, A. Nanayakkara, M. Challacombe, P. M. W. Gill, B. Johnson, W. Chen, M. W. Wong, J. L. Andres, C. Gonzalez, M. Head-Gordon, E. S. Replogle, J. A. Pople, Gaussian 98, Revision A.11.3, *Gaussian, Inc.*, Pittsburgh PA, 2002.
- [29] M. Stein, E. van Lenthe, E. J. Baerends, W. Lubitz, *J. Phys. Chem., A* **2001**, 105, 416.
- [30] P. J. Carl, S. L. Isley, S. C. Larsen, *J. Phys. Chem., A* **2001**, 105, 4563; S. C. Larsen, *J. Phys. Chem., A* **2001**, 105, 8333.
- [31] K. P. Balakrishnan, H. A. A. Omar, P. Moore, N. W. Alcock, G. A. Pike, *J. Chem. Soc., Dalton Trans.* **1990**, 2965; J. Costa, R. Delgado, *Inorg. Chem.* **1993**, 32, 5257.
- [32] W. Kabsch, *J. Appl. Cryst.* **1988**, 21, 916.
- [33] G. M. Sheldrick, *Acta Crystallogr., Sect. A* **1990**, 46, 467; G. M. Sheldrick, SHELX-97, University of Göttingen, 1997.
- [34] S. H. Vosko, L. Wilk, M. Nusair, *Can. J. Phys.* **1980**, 58, 1200.
- [35] N. Walker, D. Stuart, *Acta Crystallogr., Sect. A* **1983**, 39, 158.
- [36] L. Versluis, T. Ziegler, *J. Chem. Phys.* **1988**, 88, 322; L. Fan, T. Ziegler, *J. Chem. Phys.* **1991**, 95, 7401.
- [37] J. P. Perdew, J. A. Chevary, S. H. Vosko, K. A. Jackson, M. R. Pederson, D. J. Singh, C. Fiolhais, *Phys. Rev., B* **1992**, 46, 6671.
- [38] E. van Lenthe, A. Ehlers, E.-J. Baerends, *J. Chem. Phys.* **1999**, 110, 8943.
- [39] S. Portmann, H. P. Lüthi, *Chimia* **2000**, 54, 766.
- [40] R. E. Stratmann, G. E. Scuseria, M. J. Frisch, *J. Chem. Phys.* **1998**, 109, 8218; R. Bauernschmitt, R. Ahlrichs, *Chem. Phys. Lett.* **1996**, 256, 454; M. E. Casida, C. Jamorski, K. C. Casida, D. R. Salahub, *J. Chem. Phys.* **1998**, 108, 4439.
- [41] C. Lee, W. Yang, R. G. Parr, *Phys. Rev., B* **1988**, 37, 785; A. D. Becke, *J. Chem. Phys.* **1993**, 98, 5648.
- [42] T. H. Dunning Jr., P. J. Hay, in 'Modern Theoretical Chemistry', Ed. H. F. Shaefer III, Plenum Press, New York, **1977**, Vol. 3, p. 1–27; P. J. Hay, W. R. Wadt, *J. Chem. Phys.* **1985**, 82, 270; P. J. Hay, W. R. Wadt, *J. Chem. Phys.* **1985**, 82, 299.
- [43] R. Ditchfield, W. J. Hehre, J. A. Pople, *J. Chem. Phys.* **1971**, 54, 724; W. J. Hehre, J. A. Ditchfield, J. A. Pople, *J. Chem. Phys.* **1972**, 56, 2257; P. C. Hariharan, J. A. Pople, *Theor. Chim. Acta* **1973**, 28, 213; P. C. Hariharan, J. A. Pople, *Mol. Phys.* **1974**, 27, 209; M. S. Gordon, *Chem. Phys. Lett.* **1980**, 76, 163.
- [44] J. S. Binkley, J. A. Pople, W. J. Hehre, *J. Am. Chem. Soc.* **1980**, 102, 939.

Received February 17, 2004